Thermodynamics of strain-confined paraexcitons in Cu_2O

D. P. Trauernicht* and J. P. Wolfe

Department of Physics, University of Illinois at Urbana-Champaign, 1110 West Green Street, Urbana, Illinois 61801

A. Mysyrowicz

Group de Physique des Solides, Ecole Normale Supérieure, Université de Paris VII, Tour 23, F-75005 Paris, France

The thermodynamic behavior of long-lived paraexcitons confined to a parabolic potential well is examined. The potential well is produced by a Hertzian contact stress. A wavelength-tunable dye laser is used to create excitons directly in the potential well or at any other localized point inside the crystal. Spectral and spatial distributions of the exciton recombination luminescence are measured for cw and pulsed excitation. The possibility of Bose-Einstein condensation of these long-lived excitons is examined both theoretically and experimentally. We calculate the spectral and spatial distribution of luminescence from a gas of noninteracting particles in a three-dimensional harmonic-oscillator well. The results are markedly different for direct (no-phonon) and indirect (phonon-assisted) recombination. The calculated spectra are compared to the data for moderate cw excitation at $T_{bath} = 2-4.2$ K. Taken alone, the no-phonon spectra suggest that the excitonic gas is in the quantum regime; however, this conclusion is shown to be inconsistent with the estimated density of the gas. A consistent interpretation of all spectral and spatial distributions is possible, however, if one assumes Maxwell-Boltzmann statistics and takes into account the rapidly changing paraexciton intensity with applied stress. From time- and space-resolved studies of the orthoexciton and paraexciton luminescence, plausible causes for a saturation of paraexciton density in the strain well are deduced. First, an Auger-like recombination of colliding paraexcitons seems to limit their density—an idea supported by the observed power dependence of orthoexciton and paraexciton signals. Secondly, an anomalously slow thermalization of strain-confined paraexcitons is observed.

I. INTRODUCTION

The possibility of Bose-Einstein condensation (BEC) of excitons in semiconductors has been actively pursued for many years. The exciton, or bound electron-hole pair, is the basic electronic excited state of an intrinsic semiconductor. Its light effective mass is a favorable factor for the occurrence of BEC at moderate particle densities and relatively high temperatures. Specifically, for an ideal gas of particles, a macroscopic occupation of the ground state occurs at densities above

$$n_c = (6.2 \times 10^{15} \text{ cm}^{-3}) g (m^*/m_0) T^{3/2} ,$$

which yields $n_c = 2 \times 10^{17}$ cm^{-3} at $T = 10$ K for an exciton mass m^* equal to the free-electron mass m_0 and a degeneracy factor of $g = 1$. The observation of this quantum-statistical effect, however, has proven quite elusive, mainly due to coupling effects from exciton-exciton interactions. For example, excitons may undergo a Mott transition to an electron-hole plasma or condense into electron-hole droplets[1] before n_c is reached. Recent studies have therefore concentrated on crystals for which the Mott and/or spatial condensation densities are expected to be higher than n_c.

One excitonic system which was reported to have shown quantum-statistical effects is a gas of biexcitons in CuCl. Chase et al.[2] used two-photon absorption of a high-intensity laser to create a large initial density of biexcitons at twice the photon wave vector. When a weak density of probe particles was added to the system, a redistribution of these probe particles in k space strongly suggested the presence of a Bose condensate. Also, excitons in Ge have been reported to show quantum-statistical effects characteristic of Bose particles. For uniaxially compressed Ge in a magnetic field, Timofeev et al.[3] observed a narrowing of the exciton-luminescence line shape with increased excitation, which they interpreted as evidence for Bose-Einstein statistics. It was suggested that condensation might occur in this system at temperatures below $T \approx 1$ K.

Another crystal which has been suggested as a good candidate for the observation of excitonic BEC (Ref. 4) is Cu_2O. In this material the lowest exciton level ($n = 1$) is split into two states: a triply degenerate orthoexciton state and a nondegenerate paraexciton state lying at 12 meV lower energy. Luminescence experiments have been reported by Hulin et al.[5] showing evidence of Bose statistics for the orthoexcitons. As the excitation level was increased, both the quantum degeneracy and the temperature of the excitonic gas increased. Hulin et al. concluded that the critical density n_c for BEC was reached at their highest excitation levels and $T \approx 20$ K. A subsequent theoretical study was carried out by Haug and Kranz,[6] proposing that the data of Ref. 5 contained evidence that the particle density was in fact exceeding n_c. They noted the presence of a low-energy tail in the data which could be attributed to the scattering of excitons from a condensed fraction of particles.

In this paper we present a study of excitons in Cu_2O confined in a stress-induced parabolic potential well, with potential energy $V(r)=ar^2$. We employ a Hertzian stress configuration to confine the excitons to a controlled volume inside the crystal. This geometry looks appealing for the achievement of BEC of paraexcitons, since, in principle, one should be able to collect a high density of cold particles, away from the hotter excitation spot and from undesirable surface effects. We find that the paraexcitons exhibit a quasiequilibrium in the parabolic potential well. This is possible due to the long lifetime of paraexcitons, owing to the fact that the radiative recombination of excitons is forbidden in Cu_2O, despite the direct-band-gap structure of this material. It was previously reported that naturally grown crystals of Cu_2O exhibited paraexciton lifetimes exceeding a microsecond.[7] We employ samples of the same material for our studies.

Generally, Bose-Einstein condensation is described for an ideal gas of free particles in a region of constant potential. Significant changes are expected, however, for Bose particles in an external potential. Therefore we begin by examining theoretically the quantum-statistical behavior of bosons in a parabolic potential well. Predictions are made concerning both the spatial and energy distribution of the particles. Unlike the usual BEC for a constant potential—which is a k-*space* condensation—BEC in a harmonic-oscillator potential implies a *real-space* condensation. We show that the spatial and spectral luminescence profiles are expected to be quite different for no-phonon and phonon-assisted excitonic recombination lines.[8] The spatial distribution of phonon-assisted luminescence reflects the actual particle density.

As will be shown, interpretation of the strain-confined paraexciton luminescence spectra in terms of the above theory presents some ambiguities. The measured spectra are found to be in good agreement with the theoretical predictions and could be interpreted as being due to an ideal gas of particles in the quantum regime, close to BEC. However, calibration of the experimental particle densities in the well precludes this possibility. This discrepancy may be resolved by taking into account the strong stress dependence of paraexciton luminescence intensity and using classical statistics.

In attempting to achieve high densities of paraexcitons, we encountered some limitations associated with exciton-exciton collisions. Under increasing laser excitation, the paraexciton signal was found to behave in a very sublinear fashion. This sublinear behavior is explained in terms of an Auger-type recombination channel, where two excitons collide, resulting in the loss of one electron-hole pair and the creation of a free electron and a free hole which subsequently thermalize to form an orthoexciton. The final section of this paper characterizes these thermalization processes by time-resolved luminescence measurements.

II. BOSE STATISTICS IN A PARABOLIC WELL

We wish to predict the luminescence spectrum and spatial distribution of excitons that are confined in a three-dimensional harmonic-oscillator potential, $V(r)=ar^2$. If it is assumed that they behave as a classical gas and that the matrix element for radiative recombination is independent of wave vector and spatial position, the spatial profile can be obtained quite simply. For a classical gas, the internal chemical potential is $\mu_{int}=k_BT\ln(n/n_q)$, where $n=n(r)$ is the density and $n_q=(m^*k_BT/2\pi\hbar^2)^{3/2}$ is the quantum density.[9] The total chemical potential μ is the sum of the internal and external chemical potential ($\mu_{ext}=ar^2$). Since $\mu=$const in the potential well, one obtains

$$k_BT\ln[n(0)/n_q]=k_BT\ln[n(r)/n_q]+ar^2 , \qquad (1)$$

which has the solution

$$n(r)=n(0)\exp(-ar^2/k_BT) . \qquad (2)$$

On way of obtaining the luminescence line shape under the above assumptions is to note that a harmonic oscillator has energy levels $E_s=(s+\frac{3}{2})\hbar\omega$ with $\omega=(2a/m^*)^{1/2}$ and $s=1,2,\ldots,\infty$. Each level has a degeneracy of $(s+1)(s+2)/2$. Since the energy levels are equally spaced, the density of states is given by the degeneracy. For typical experiments $\hbar\omega\approx10^{-9}$ eV $\ll k_BT$, implying that most particles are in states $s\gg1$. The density of states then varies as E^2. Assuming a Maxwell-Boltzmann population of these states, the luminescence line shape is predicted to be

$$I(E)\propto E^2\exp(-E/k_BT) . \qquad (3)$$

As the exciton gas approaches degeneracy $(n\rightarrow n_q)$, the above equations do not hold. Indeed, there is no closed-form expression for the chemical potential of degenerate Bose gas as a function of density. One method of calculating the spatial profile is to sum over the probability distribution for harmonic-oscillator wave functions weighted by the probability of occupation of the state,

$$\{\exp[(E_s-\mu)/k_BT]-1\}^{-1} .$$

Alternatively, one can consider the confined gas as a sum of small volumes with nearly uniform density, which is the approach we now take. The results depend upon whether the observed recombination light is due to a no-phonon or phonon-assisted transition. The no-phonon transition is constrained (locally) to the $K=0$ selection rule, whereas the phonon-assisted transition can sample a full range of exciton wave vectors.

A. Phonon-assisted transitions

Suppose that the spatial profiles and luminescence line shapes are given by the sum of local line shapes, which are dependent on the spatial position. For phonon-assisted recombination in which the matrix element is assumed independent of wave vector, the local line shape is given by

$$I_{loc}(E,r)\propto\frac{\mathscr{D}_{loc}(E,r)}{\exp[(E_{loc}-\mu_{loc})/k_BT]-1} , \qquad (4)$$

where $\mathscr{D}_{loc}(E,r)=(E-ar^2)^{1/2}$ is the local density of states, $E_{loc}=E-ar^2$ is the local kinetic energy, and $\mu_{loc}=\mu-ar^2$ is the local internal chemical potential. The

total chemical potential μ is independent of position r. The spatial profile is obtained by integrating Eq. (4) over energy. Note that E must be greater than αr^2. This yields

$$I(r) \propto \sum_{n=1}^{\infty} \frac{\exp[-n(\alpha r^2 - \mu)/k_B T]}{n^{3/2}} . \tag{5}$$

If the system is not degenerate (μ is large and negative), this reduces to the form of Eq. (2), because only the first term in the sum will contribute. Similarly, the luminescence line shape is obtained by integrating Eq. (4) over all space. This yields

$$I(E) \propto \frac{E^2}{\exp[(E-\mu)/k_B T]-1} , \tag{6}$$

which reduces to the form of Eq. (3) for a nondegenerate system.

Shown in Fig. 1(a) is Eq. (6) for various values of μ at $T=2$ K. In Fig. 1(b) is Eq. (5) integrated over the y-z
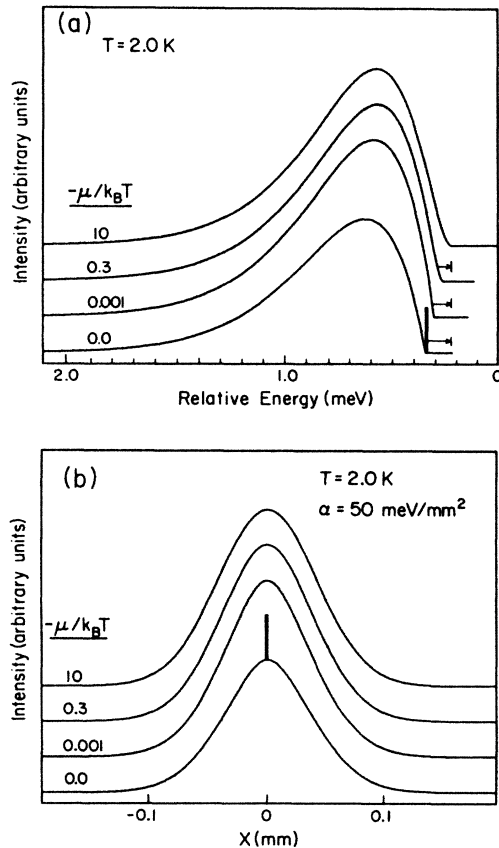

FIG. 1. Theoretical predictions for the luminescence line shape [panel (a)] and the spatial profile [panel (b)] of a phonon-assisted emission line from excitons confined to a parabolic potential well. The different curves are for varying degrees of quantum degeneracy. Note the slight change that occurs in both the luminescence line shape and the spatial profile when some quantum degeneracy is assumed. The bottom trace in each panel schematically includes macroscopic occupancy of the ground state when $\mu = 0$.

plane ("slit scans") for the same values of μ and T as above. These calculations display very little change in the spectral line shape or the spatial profile when degeneracy is assumed. The width of the spectral line shape does not change noticeably, but the peak of the distribution does shift somewhat to lower energy. The spatial profile narrows only slightly.

Because the ground state is excluded in the above calculations, a schematic representation of its effect is shown in the bottom traces of Figs. 1(a) and (b). The ground-state population is simply included as a spike on the low-energy edge of the spectrum and in the center of the parabolic well, respectively. This illustrates an important aspect of strain-confined excitons: BEC into the lowest-energy level (the harmonic-oscillator ground state) implies a *spatial* condensation. This is unlike the constant-potential case, for which there is a condensation to $K=0$ in *wave-vector* space, not a spatial condensation.

A proper calculation of the particle distribution with the inclusion of the ground state needs to be done. Specifically, the low-energy spike on the spectral line shape could be broadened due to interactions in the condensate. The recombination event may involve simultaneous emission or absorption of a coherent ground-state excitation, as pointed out by Haug and Kranz.[6]

The above analysis indicates that for phonon-assisted transitions, which sample the entire exciton-energy distribution, the approach to quantum statistics will not be easily seen. Only when the system reaches the BEC density and there is a partial condensate will there be definite signs of degeneracy.

B. Direct transitions

In the case of a direct-gap semiconductor, no-phonon transitions are also observable. No-phonon transitions sample the states near $K=0$, specifically those with wave vectors equal to the emitted photon wave vector. The photon momentum is usually small compared to the spread of momentum in the system of particles. One can calculate the luminescence distributions by summing local line shapes again. Assuming that the no-phonon transition is vertical (i.e., ignoring the photon momentum), the local line shape is given by

$$I_{loc}(E,r) \propto \frac{\delta(E_{loc})}{\exp[(E_{loc}-\mu_{loc})/k_B T]-1} , \tag{7}$$

where the δ-function picks out the local zero-kinetic-energy state, with the number of particles in this state being given by the Bose factor. To obtain the spatial profile, one integrates Eq. (7) with respect to energy. This is quite easily done because of the δ function, and one obtains

$$I(r) \propto \frac{1}{\exp[(\alpha r^2-\mu)/k_B T]-1} . \tag{8}$$

Equation (8) reduces to the form of Eq. (2) for a nondegenerate system (μ large and negative). The luminescence line shape is obtained by integrating Eq. (7) over all space, which yields

$$I(E) \propto \frac{E^{1/2}}{\exp[(E-\mu)/k_B T]-1} . \tag{9}$$

The line shape is significantly different from Eq. (6) in that Eq. (9) has an $E^{1/2}$ multiplier while Eq. (6) has an E^2 multiplier.

Shown in Fig. 2(a) is Eq. (9) for various values of μ at $T=2$ K. In Fig. 2(b) is Eq. (8) integrated over the y-z plane for the same values of μ and T. In this case of no-phonon transitions, there is a significant change in the luminescence line shape and spatial profile as the system becomes degenerate. This is due to the local $K=0$ selection along with the fact the density is higher in the center of the well, implying higher degeneracy there. A more degenerate local line shape (remember $\mu_{loc}=\mu-ar^2$) has a larger number of particles in the $E_{loc}=0$ state. This effect implies a sharper measured spatial profile than for the phonon-assisted spatial distribution, which samples all K vectors. Shown as the bottom trace in each part of Fig. 2 is schematically what would be expected for a partially condensed system. Both Eqs. (8) and (9) contain singularities when $\mu=0$. These are indicated by the arrows pointing upward.
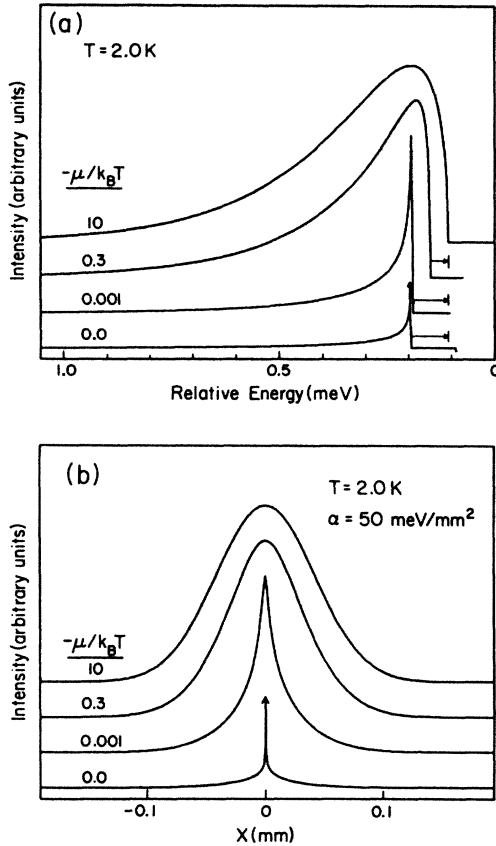

FIG. 2. Theoretical predictions for the luminescence line shape [panel (a)] and spatial profiles [panel (b)] of a no-phonon emission line from excitons confined to a parabolic potential well. The different curves are for varying degrees of quantum degeneracy. There are significant changes in both the luminescence line shape and the spatial profile when some degeneracy is assumed. The bottom trace in each panel schematically includes macroscopic occupancy of the ground state when $\mu=0$. Both these degenerate traces have singularities which are shown as the arrows pointing upward.

From this analysis of the no-phonon line shape and spatial profiles, it appears that the no-phonon line should be useful when searching for Bose statistical effects for excitons confined in a parabolic well. There are gradual changes in the line shape and spatial profile which signal the onset of quantum degeneracy, in contrast to the phonon-assisted transitions. However, the phonon-assisted transition may provide a more definitive identification of condensation.

C. Contrasts with constant-potential case

For BEC in a harmonic-oscillator well, the parameter which determines the occurrence of condensation at a given temperature is the *total number* of particles in the well rather than the *density*. This is seen by calculating the total number of particles in the well,

$$N = g \sum_s \frac{(s+1)(s+2)/2}{\exp\{[(n+\frac{3}{2})\hbar\omega-\mu]/k_BT\}-1} , \tag{10}$$

where g is an additional degeneracy factor (e.g., a spinlike degeneracy). Setting $\mu=0$ to obtain the maximum number that can be held in the excited states in equilibrium, assuming $s \gg 1$ as before, and changing the sum over s to an integral over ds, one obtains

$$N_c = g(1.202)(k_BT/\hbar\omega)^3 . \tag{11}$$

This critical number can be "converted" to a critical density by dividing by the volume of the well occupied by excitons, as determined by the full width at half maximum (FWHM) of the spatial distribution; i.e., $n_c^{well}=N_c/\Omega$, with the effective volume given by

$$\Omega = (\pi/6)(2.77k_BT/\alpha)^{3/2} . \tag{12}$$

The factor 2.77 comes from choosing the FWHM of the density profile rather than, say, the $1/e$ point. The simple Gaussian spatial profile result is assumed because there is only a minor change in the width of the spatial distribution of the particles in the excited states when approaching Bose degeneracy, as shown above. [The phonon-assisted transition, Fig. 1(b), mimics the local density, whereas the no-phonon transition, Fig. 2(b), does not.] This results in a critical density given by

$$n_c^{well}(T)=0.176\frac{gm^{3/2}}{\hbar^3}(k_BT)^{3/2} . \tag{13}$$

Note that the well parameter α does not appear in Eq. (13). This may be compared with the result for "particles in a box," which is[9]

$$n_c^{free}(T)=0.166\frac{gm^{3/2}}{\hbar^3}(k_BT)^{3/2} . \tag{14}$$

There is little difference between the densities in Eqs. (13) and (14). For this reason, one can still speak of a critical density for BEC of excitons in a parabolic well, with this density being the same as that for "free" particles.

III. STRAIN CONFINEMENT OF PARAEXCITONS

To produce a parabolic well inside the crystal, an inhomogeneous stress is applied to the sample by pressing a

rounded plunger against one face of the sample. This Hertzian stress geometry has been described elsewhere for the indirect-gap semiconductors Si and Ge.[10,11] A maximum of shear stress is produced at a finite distance into the sample. As discussed below, the excitons are attracted to this shear-stress maximum (SSM) and confined there. The parabolic dependence of the external potential acting on the excitons comes about from a Taylor expansion of the stress distribution near the SSM.

Excitons are attracted to a SSM if their energy is lowered by the application of a shearing stress. For paraexcitons in Cu_2O, the application of an uniaxial stress along a fourfold axis lowers their energy as reported in an earlier paper.[12] Waters et al.[13] have shown through second-order perturbation theory that the paraexcitation energy as a function of stress can be expressed in the following form:

$$E_{para} = A + B\sigma - C\sigma^2 , \qquad (15)$$

where σ is the magnitude of the uniaxial stress. Each

term is easily identified. A is the unperturbed paraexciton energy, $B\sigma$ is due to the dilational term in the strain Hamiltonian, and $C\sigma^2$ is from a term of lowered symmetry in the strain Hamiltonian. It is the dominance of the $C\sigma^2$ term at high applied stresses that makes the SSM an energy minimum for the paraexcitons because this term incorporates nondilational (shear) strains.

Shown in Fig. 3 are two spectra. The lower trace is a photoluminescence spectrum from a crystal with no stress applied and excited by an argon-ion laser. X_0 denotes orthoexciton no-phonon line; other lines are optical-phonon replicas of the orthoexciton line and are identified by the symmetry of the phonon emitted. Also observed is a phonon replica of the paraexciton labeled X_P-Γ_{25}^-. The upper trace is a spectrum taken from the SSM at an approximate stress of 3.6 kbar. Note that the wavelength scale is shifted. An additional line appears under the application of a symmetry-lowering stress and is identified as the no-phonon line of the paraexciton,[14] X_P. This spectrum is obtained by resonantly pumping (with a tunable dye laser) the down-shifted phonon-assisted orthoexciton absorption band at a spatial position "below" the well. The longer-lived paraexcitons drift into the well. The appearance of a relatively small orthoexciton signal, in comparison to the much stronger no-phonon paraexciton line, comes from orthoexcitons created by Auger decay of paraexcitons in the well, as discussed later.

The dependence of the paraexciton energy (position of the X_P line) on applied stress is shown in Fig. 4. The
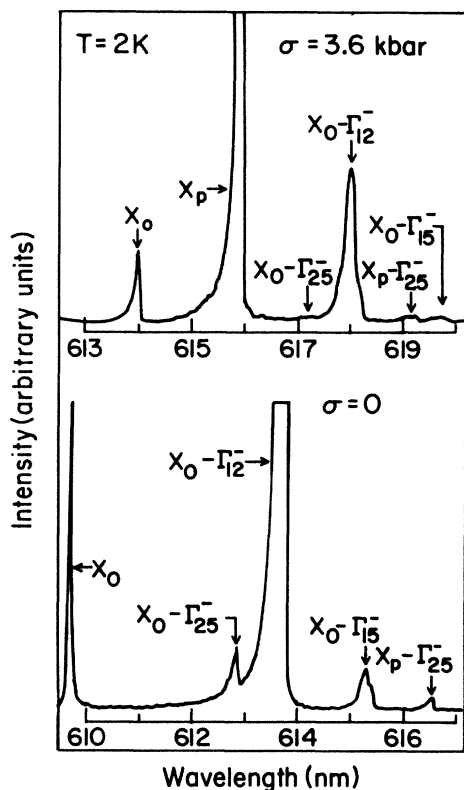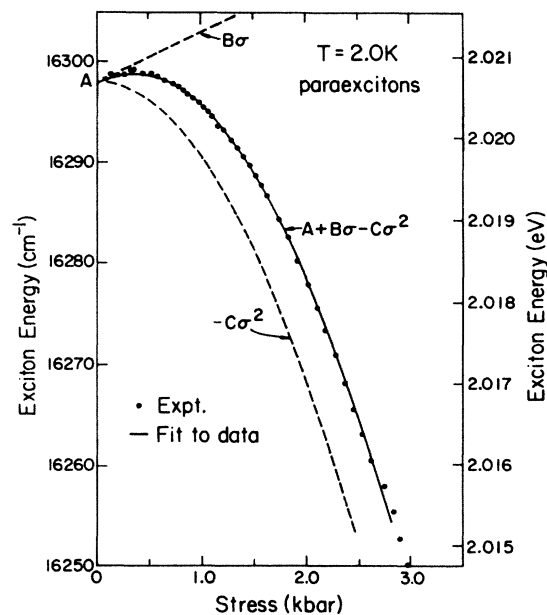

FIG. 3. Luminescence spectra taken with no stress applied to the crystal (lower trace), and with a stress of about 3.6 kbar at the shear-stress maximum (upper trace). Note the different wavelength scales for the two spectra. X_0 is the no-phonon orthoexciton emission and the other lines are phonon replicas of the orthoexciton labeled by the symmetry of the optical phonon emitted, with the exception of the X_p-Γ_{25}^- line, which is the phonon-assisted paraexciton emission. A new line appears when uniaxial stress is applied to the crystal—the no-phonon paraexciton line labeled X_p. This line is cut off at about $\frac{1}{8}$ its maximum intensity and the x_0-Γ_{12}^- line is cut off at about $\frac{1}{3}$ its maximum intensity.

FIG. 4. Energy position of the paraexciton as a function of applied stress, σ. The data were obtained by using the measured energy shift of the orthoexciton line as the stress calibrator. The fit to the orthoexciton-versus-stress data given in Ref. 13 was used as the calibrating curve. The solid curve is a fit of Eq. (15) to the data with the values $A = 16298$ cm^{-1}, $B = 4.96$ cm^{-1}kbar^{-1}, and $C = 7.36$ cm^{-1}kbar^{-2}. The contribution of the separate terms of Eq. (15) are shown as the dashed curves. The dominance of the $C\sigma^2$ term at high stresses makes the shear-stress maximum an energy minimum for the paraexcitons.
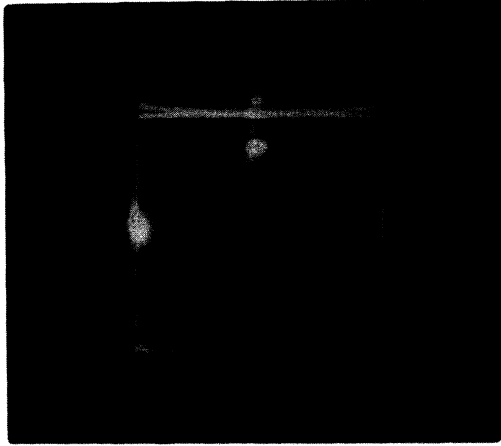
FIG. 5. Photograph of a Cu_2O crystal with stress applied by a glass plunger. An argon-ion laser excites the surface of the sample. The created excitons drift in the stress gradient to the shear-stress maximum where they are confined. This region is the bright spot near the top of the sample. The luminescence seen above the sample is due to a reflection from the glass plunger. The sample dimensions are $1.5 \times 1.5 \times 1.5$ mm³.

stress is calibrated using the measured energy position of the down-shifted orthoexciton line and the data of Waters et al.,[13] who measured the orthoexciton energy as a function of applied uniaxial stress. The solid curve is a fit of Eq. (15) to the data, yielding the values of A, B, and C given in the figure caption. The initial rise of the paraexciton energy is due to the $B\sigma$ term, but the $C\sigma^2$ dominates at high stresses to give an energy minimum at the SSM.

In the present experiment, a glass plunger with radius of curvature ≈ 2.5 cm was pressed against a (100) face of a Cu_2O crystal with dimensions $1.5 \times 1.5 \times 1.5$ mm³. Figure 5 is a photograph of the stressed crystal at $T = 1.5$ K with Ar⁺-laser surface excitation ($\lambda = 5145$ Å). The bright spot just below the top of the crystal is luminescence due to excitons confined near the SSM. In this case, the excitons must drift about 1 mm from the surface into the potential well. The drift path is barely visible. The luminescence above the sample is due to a reflection from the glass plunger.

IV. LUMINESCENCE LINE SHAPES AND SPATIAL PROFILES

To obtain the proper luminescence line shape of excitons confined to parabolic well, one must collect light from all parts of the well while maintaining high spectral resolution. In this work, a method of "dynamic spatial integration" is used to obtain such a luminescence spectrum. A $6\times$ magnified image of the sample is projected onto the entrance slit of a 1-m spectrometer. (See Fig. 1 of Ref. 15.) A 1-mm-wide aperture is used to select spatially the well area in the vertical dimension. The size of the entrance slit is kept small in order to have a high spectral resolution; but this narrow slit could sample only a fraction of the well. To integrate over all portions of the

well, the image of the sample is scanned horizontally across the slit at a (5–10)-Hz repetition rate using a triangular waveform to drive the galvanometer, so that there is equal integration times for all portions of the well. The total integration time is ≥ 1 sec, so that many passes of the image are sampled at each wavelength.

The next data to be described have been obtained by pumping with a tunable dye laser the orthoexciton "below" the well, resulting in subsequent particle drift upwards into the well (see inset of Fig. 6). The wavelength of the dye laser is tuned to the low-energy edge of the locally down-shifted orthoexciton phonon-assisted absorption band, resulting in an excited region of the crystal about 0.5 mm in length. Incident laser power is low, about 0.3 mW cw, with about 10% absorption. Each absorbed photon is converted into an orthoexciton and a 110-cm⁻¹ optical phonon. The orthoexcitons rapidly down-convert to paraexcitons,[7,16] which then drift upwards into the well.

In Fig. 6 no-phonon paraexciton line shapes taken at three different temperatures are displayed. Also shown are fits of Eq. (9) to the data assuming nondegeneracy $[I(E) \propto E^{1/2}\exp(-E/k_BT)]$ and using temperature as the main fit parameter. (The two other fit parameters are
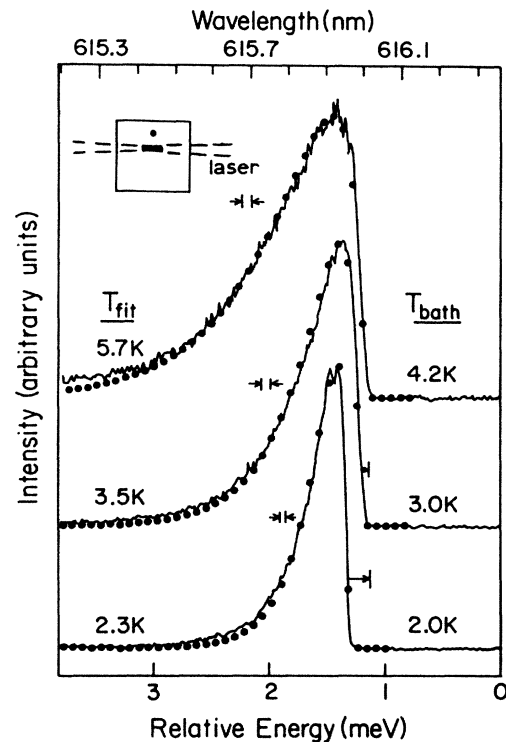

FIG. 6. No-phonon paraexciton luminescence line shapes for three bath temperatures taken using "dynamic spatial integration" of luminescence emitted from the potential well as explained in the text. The fits to the data (solid circles) are the nondegenerate limit of Eq. (9) [i.e., $E^{1/2}\exp(-E/k_BT)$] convolved with the resolution function shown at the left of each trace. The resultant fit temperatures are given at the left and the bath temperatures are given at the right. The magnitude of the applied stress was about 3.6 kbar.

peak intensity and energy offset.) Both fit and bath temperatures are given.

Phonon-assisted paraexciton line shapes were also taken under identical excitation conditions. Shown in Fig. 7 are phonon-assisted line shapes taken at the same bath temperatures as in Fig. 6. These spectra are difficult to obtain because of the weak signal and the proximity of phonon-assisted orthoexciton lines. The applied stress for all the data described in this section ($\sigma \approx 3.6$ kbar) is chosen so that the paraexciton phonon-assisted line is optimally separated from the nearby orthoexciton phonon-assisted lines. Also shown in Fig. 7 are fits of Eq. (6) to the data assuming nondegeneracy [i.e., $I(E) \propto E^2 \exp(-E/k_B T)$]. Again, temperature is the main fit parameter. First, consider the bottom spectrum in Fig. 7. The fit temperature of 3.0 K is higher than the fit temperature of 2.3 K for the no-phonon line. There is a similar discrepancy for the middle and top spectra in Figs. 6 and 7. Due to the ambiguity of the baseline for the phonon-assisted line at higher temperatures, the tempera-
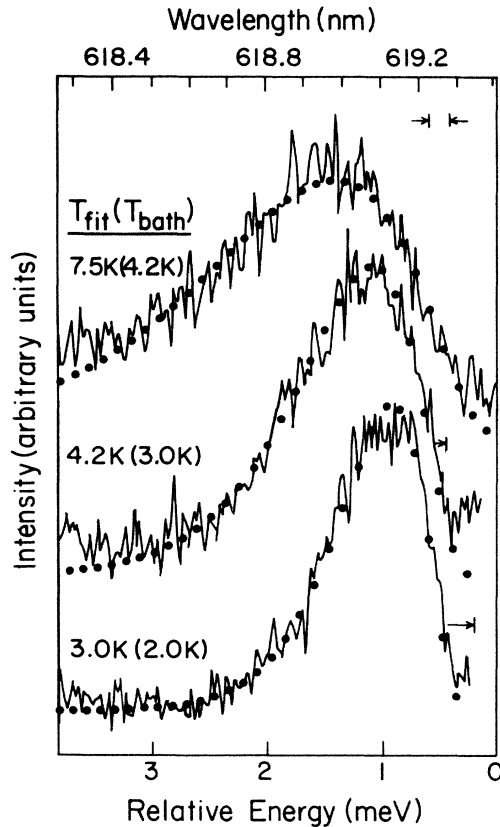
ture derived from the top spectrum in Fig. 7 has some uncertainty (about ± 1.5 K).

Clearly, the procedure used for fitting the data of Figs. 6 and 7 is inadequate, since the direct and phonon-assisted emission lines should yield the same temperature, which is not the case here. What could be causing a difference between the fit temperatures of the no-phonon and phonon-assisted spectra? One possibility is to introduce quantum degeneracy, which will affect the no-phonon line shape much more than the phonon-assisted line, as explained in the preceding section. Shown in Fig. 8 are the same data as in Fig. 6, but the theoretical fits to the data (the solid dots) are obtained from Eq. (9), assuming some degree of degeneracy. The temperatures introduced for bath temperatures ≤ 3 K are fixed by the phonon-assisted line-shape fits of Fig. 7. The chemical potential is then the main fitting parameter in Fig. 8. The temperature and chemical potential for the theoretical fits are given at the left of each spectrum. The top spectrum is fit by allowing both T and μ to vary. The fit temperature turns out to be the same as that shown for the top spectrum of Fig. 7. For comparison, nondegenerate line shapes with the same

FIG. 7. Phonon-assisted paraexciton luminescence line shapes for the same bath temperatures as Fig. 6 taken using "dynamic spatial integration" of luminescence emitted from the potential well. The fits to the data (solid circles) are the nondegenerate limit of Eq. (6) [i.e., $E^2 \exp(-E/k_B T)$] convolved with the resolution function shown in the upper right-hand corner. Fit temperatures are shown at the left. The "fit" temperature of 7.5 K for the top trace is a bit uncertain due to ambiguous baseline determination, which is a result of nearby orthoexcitation phonon-assisted lines. The determination of this temperature is explained in the text.
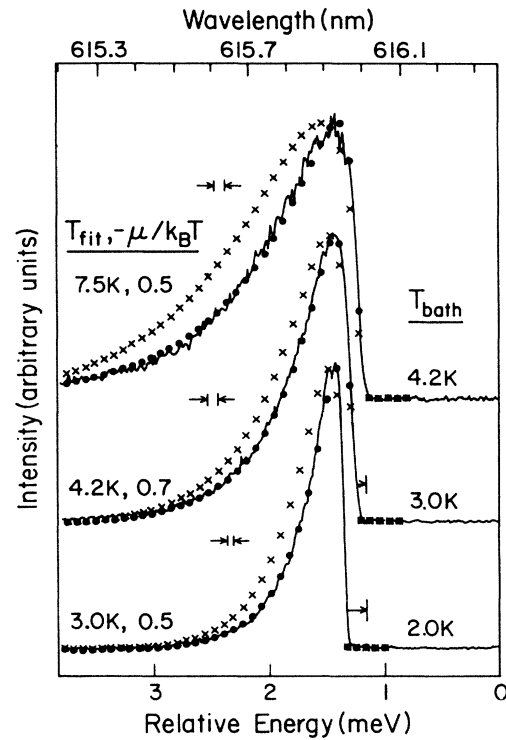
FIG. 8. No-phonon paraexciton luminescence line shapes again, the same data as in Fig. 6. These fits to the data (solid circles) are Eq. (9) assuming some quantum degeneracy. The fit temperatures for the lower two spectra were fitted at the values obtained for the phonon-assisted line shapes (see Fig. 7) and the chemical potential μ was allowed to vary. The resulting values of μ are given at the left as a fraction of $k_B T$, where T is the fit temperature. For the upper spectrum, both T and μ were varied for the best fit. Shown as the $\times$'s is the corresponding nondegenerate line shape with the same temperature as the fit temperature given. The assumption here of quantum degeneracy is actually invalid as explained in the text.

effective temperature as for the degenerate fits are also shown in Fig. 8.

So far, the assumption of Bose degeneracy would explain both the no-phonon and phonon-assisted luminescence line shapes. The next question is whether the exciton densities are high enough to justify the assumption of Bose degeneracy. In order to estimate the density, the relation $N = G\tau_I$ is used, where N is the number of excitons, G is the generation rate of excitons, and τ_I is the initial decay time of the excitons. Knowing the incident power of about 0.3 mW with 10% absorption and an initial decay time of order 0.3 μsec, then assuming 100% exciton-creation and well-collection efficiency, one obtains the estimated number of excitons in the well to be $\approx 2.8 \times 10^7$. The volume occupied is obtained from the measured spatial FWHM, here about 100 μm. This gives a volume of $\approx 5 \times 10^{-7}$ cm^3. The estimated exciton density is then $\approx 5.6 \times 10^{13}$ cm^{-3}. This is more than 3 orders of magnitude below the critical density obtained from Eq. (13), which gives $n_c \approx 10^{17}$ cm^{-3} at $T = 2$ K. For this reason, we are lead to the conclusion that the existence of Bose degeneracy at this low excitation level is highly unlikely. Thus, the above analysis illustrates the danger in using only spectroscopic information to determine the degeneracy of the excitonic system.

What could be an alternate explanation? A plausible explanation is as follows: Consider the assumptions made in deriving the expressions for the line shapes and spatial profiles. The matrix element was assumed independent of spatial position. Yet it is known that the intensity of the no-phonon paraexciton line is dependent on the applied stress. Kreingol'd and Makarov[17] reported the intensity of the no-phonon paraexciton line to behave as σ^2, where σ is the magnitude of the applied stress. The paraexcitons in a stress-induced potential well do experience a range of stresses. The intensity of the phonon-assisted line is not greatly affected by stress; hence, it is assumed to have a constant matrix element over the range of stresses in the well.

However, the σ^2 intensity dependence can affect the no-phonon luminescence line shape emitted from the well. Equation (7) must be modified to include the spatial dependence of the matrix element. Let the intensity of the paraexciton be given by $I_p = \beta\sigma^2$. If the magnitude of the stress at the SSM is σ_0, then the stress distribution around the SSM can be expressed as

$$\sigma - \sigma_0 = -Sr^2 , \qquad (16)$$

where S is the second derivative of stress with respect to r, evaluated at $r = 0$ (the center of the well). Expanding I_p about σ_0, one obtains

$$I_p = \beta\sigma_0^2 + 2\beta\sigma_0(\sigma - \sigma_0) + 2\beta(\sigma - \sigma_0)^2 . \qquad (17)$$

Substituting Eq. (16) into Eq. (17), one obtains the spatial dependence of the paraexciton intensity (which is proportional to the square of the matrix element). Equation (7) now becomes

$$I(E,r) \propto \frac{(\beta\sigma_0^2 - 2\beta\sigma_0 Sr^2 + 2\beta S^2 r^4)\delta(E_{\text{loc}})}{\exp[(E_{\text{loc}} - \mu_{\text{loc}})/k_B T] - 1} . \qquad (18)$$

Integrating over all space now yields

$$I(E) \propto \frac{E^{1/2} - 2\eta E^{3/2} + 2\eta^2 E^{5/2}}{\exp[(E - \mu)/k_B T] - 1} , \qquad (19)$$

where $\eta = S/\sigma_0\alpha$. The second and third terms in the numerator represent the correction to Eq. (9) due to the stress dependence of the intensity. One can estimate the parameter η knowing that $S \approx \sigma_0/z_0^2$, where z_0 is the distance of the SSM from the top surface[18] (see Fig. 5). Using the values $\sigma_0 = 3.6$ kbar and $z_0 \approx 0.25$ mm, one gets $S \approx 57$ kbar/mm^2. With a typical $\alpha \approx 50$ meV/mm^2, this yields $\eta \approx 0.3$ meV^{-1} or 300 eV^{-1}. Equation (19) is shown as the solid curve in Fig. 9 for $T = 7.5$ K and $\eta = 300$ eV^{-1} and assuming classical statistics ($|\mu| \gg k_B T$). The other curves are the components of this line shape corresponding to the different terms in Eq. (19) taken separately with the occupation probability factor, $\exp(-E/k_B T)$. They show that the stress-dependent intensity correction is significant. The open circles are the $E^{1/2}$ term, the open squares are the $E^{3/2}$ term, and the crosses are the $E^{5/2}$ term. The relative magnitudes of the plots correspond to the relative multipliers for each term. Comparing the solid curve with the open-circle curve, one sees that Eq. (19) is narrower than Eq. (9) for a given temperature.

Shown in Fig. 10 are the no-phonon line shapes with Eq. (19) fitted to the data. Both the temperature and the parameter η are allowed to vary initially. It is found that $\eta = 300$ eV^{-1} gives fairly consistent results for all the bath temperatures, with the fit temperature close to the phonon-assisted line shapes at the lower temperatures. Slight differences between the fit temperature of the no-
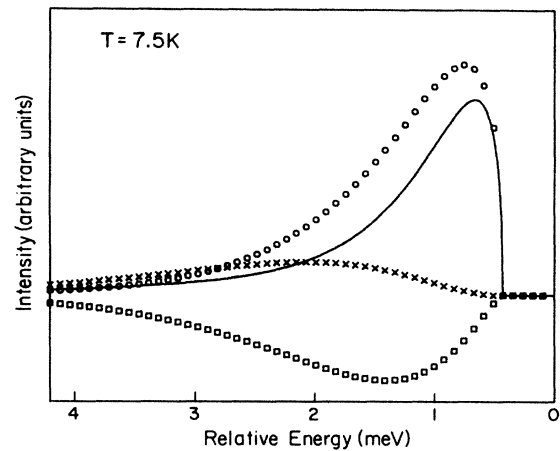

FIG. 9. Luminescence line shape for the no-phonon paraexciton line taking into account the variation in emission intensity with stress. Maxwell-Boltzmann statistics ($|\mu| \gg k_B T$) is assumed. The dashed curves (circles, squares, and $\times$'s) are the components of the line shape as given by the different terms in Eq. (19), with an inverted curve indicating a negative contribution. The resultant line shape is shown as the solid curve. A temperature of 7.5 K was used with the parameter $\eta = 300$ eV^{-1}. Note that this line shape is narrower at a given temperature than the line shape given in Eq. (9).
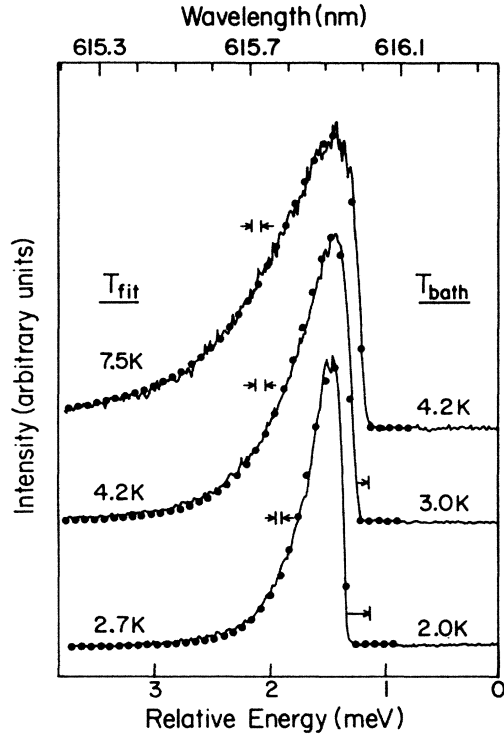
FIG. 10. No-phonon paraexciton luminescence line shapes again, the same data as in Fig. 6. The fits to the data (solid circles) are Eq. (19) convolved with the resolution function shown at the left of each curve and $|\mu| \gg k_B T$. A single value of $\eta = 300$ eV^{-1} was used for all fits. Temperature was allowed to vary somewhat, but good fits were obtained with temperatures the same as or very close to the fit temperatures obtained from the phonon-assisted line shapes (see Fig. 7).
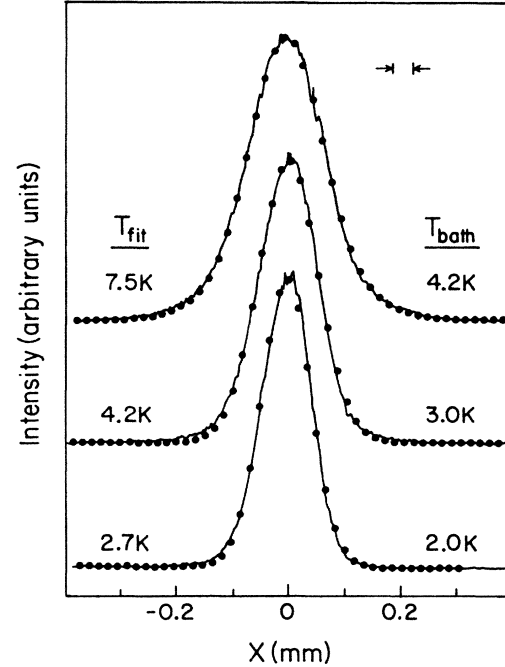

FIG. 11. Spatial profiles of the no-phonon paraexciton line at the same bath temperatures as Fig. 10. The fits to the data (solid circles) are Eq. (21) with the same value $\eta = 300$ eV^{-1} and the same fit temperatures as those in Fig. 10. Shown in the upper right-hand corner is the estimated spatial resolution.

phonon and the phonon-assisted line shapes still exist for bath temperatures of 2 K and below. Basically, the spectral inconsistencies seem to be resolved by including the stress dependence of the no-phonon luminescence intensity. The Maxwell-Boltzmann statistics used are consistent with the estimated density.

Now consider the spatial profile taking into account the stress-dependent intensity of the no-phonon line. One must integrate Eq. (18) with respect to energy. This yields

$$I(r) \propto \frac{1 - 2\eta\alpha r^2 + 2\eta^2\alpha^2 r^4}{\exp[(\alpha r^2 - \mu)/k_B T] - 1} . \quad (20)$$

Assuming nondegeneracy, and the integrating over the y-z plane, one obtains

$$I(x) \propto \left\{ 1 - 2\left[\eta\alpha\left(x^2 + \frac{k_B T}{\alpha}\right)\right] \right.$$
$$\left. + 2\left[\eta\alpha\left(x^2 + \frac{k_B T}{\alpha}\right)\right]^2 \right\} \exp(-\alpha x^2/k_B T) . \quad (21)$$

Shown in Fig. 11 are spatial profiles of the no-phonon line taken at the same bath temperatures as the above described line shapes. The solid dots are fits of Eq. (21) to the data using $\eta = 300$ eV^{-1} and the temperatures from

the fits in Fig. 10. The well parameter α was allowed to vary. It is found that $\alpha = 53$ meV/mm^2 gives the best fit to spatial distributions at all temperatures. One sees that there is excellent agreement and consistency among the spatial profiles and the luminescence line shapes. Note that for all the data described above, the same values of η and α are used for all temperatures.

One conclusion that must be drawn from this data is that the paraexcitons in the parabolic well do not seem to thermalize completely with respect to the lattice within their lifetime. This is in contrast with data taken on crystals under zero applied stress, where thermalized paraexciton line shapes are observed even for much higher excitation conditions. Notice that the fit temperature in Fig. 10 is always greater than the bath temperature, and the disparity decreases as the bath temperature is lowered. This is opposite to what one might expect based on the fact that the phonon scattering time increases as temperature is lowered, which should result in longer thermalization times at lower temperatures. There is, however, an additional "thermalization" that must take place in this case, i.e., a spatial thermalization. The paraexcitons must fill the well volume, creating an equilibrium spatial distribution under the application of this external potential. At the higher temperatures, the equilibrium size of the spatial profile is larger than at low temperatures [see Eqs. (2) and (12)]. Also, the diffusivity of the paraexcitons at high temperatures is much smaller than at the low temperatures;[15] therefore, it takes longer for the excitons to fill the well at the higher temperatures. These factors would pro-

duce a larger disparity between the fit and bath temperatures at the higher bath temperatures.

V. KINETICS OF ORTHOEXCITONS AND PARAEXCITONS

The previous data were obtained at a relatively low level of excitation, an absorbed power of ≈ 0.03 mW. To increase the density of excitons, one naturally should increase the laser intensity. In so doing, we discovered that the paraexciton intensity (assumed proportional to the number of particles) increased in a sublinear fashion. Another puzzling observation was that an orthoexciton luminescence signal emanated from the well region even when the excitation point was at a considerable distance away from the well (see Fig. 3). The short orthoexciton lifetime (≈ 3 nsec) (Refs. 7 and 16) should preclude travel over macroscopic distances. Also, thermal population of the orthoexciton level should be negligibly small: $\exp(-\Delta E/k_B T) \approx 7 \times 10^{-21}$ for an ortho-para splitting $\Delta E \approx 8$ meV and temperature $T = 2$ K.

Shown in Fig. 12 is the relative intensity of both orthoexciton and paraexciton luminescence from the well as a function of absorbed laser power P. The excitation configuration is the same as that described in the preceding section—the laser absorption occurs in a region separated from the well by about 400 μm and the excitons drift into the well. The intensity of the orthoexciton was obtained from the 110-cm^{-1} optical-phonon replica (X_0-Γ_{12}^-). Notice the strongly sublinear behavior of the paraexciton intensity at high excitation: it is nearly a $P^{1/4}$ dependence. The laser beam was mechanically chopped with a 4% duty factor at the higher powers to avoid crystal heating. The power dependence of the orthoexciton intensity is significantly different from that
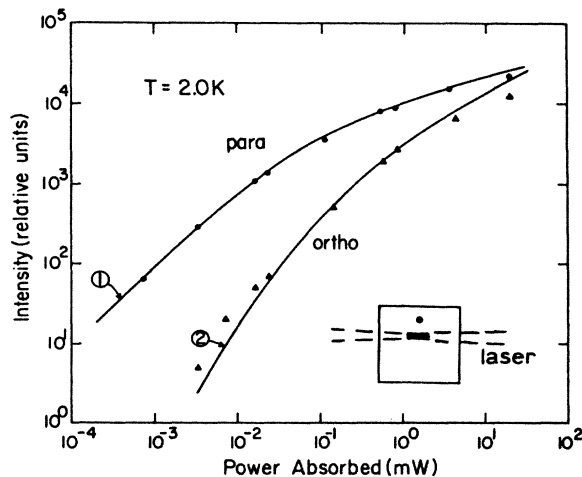

FIG. 12. Intensity of the no-phonon paraexciton line and the Γ_{12}^- phonon replica of the orthoexciton as a function of absorbed laser power. The excitation configuration is shown in the inset. The laser is absorbed in a region below the potential well and the excitons drift upwards into the well (shown as the solid circle near the top of the sample). The solid curves are fits of Eq. (25) to the data.

of the paraexciton. In fact, the orthoexciton intensity seems to behave approximately as the square of the paraexciton intensity.

The power dependences of the orthoexciton and paraexciton intensities can be modeled by rate equations. There are *two* spatial regions that must be considered: the region where the laser light is absorbed and the region of potential well. First, consider the pumped region away from the well. Let N_0 and N_p be the number of orthoexcitons and paraexcitons in this region. The orthoexcitons are generated at a rate G determined by the number of photons absorbed per unit time t. The resulting equations are

$$\frac{\partial N_p}{\partial t} = -\frac{N_p}{\tau_p} + \frac{N_0}{\tau_{DC}} - aN_p^2 \tag{22a}$$

and

$$\frac{\partial N_0}{\partial t} = G - \frac{N_0}{\tau_{DC}} + \frac{a}{2}N_p^2 , \tag{22b}$$

where τ_p is the radiative lifetime of the paraexciton, τ_{DC} is the down-conversion time for the creation of paraexcitons from orthoexcitons. The aN_p^2 term is due to an Auger decay process[19] in which two paraexcitons collide, resulting in the loss of one electron-hole pair and the ionization of one paraexciton into a free electron and a free hole; therefore, the two colliding paraexcitons are lost in this process. The free electron and free hole are assumed to form an orthoexciton; hence, this is a source of orthoexcitons [third term on the right-hand side of Eq. (22b)] but has the weighting $\frac{1}{2}$ in the equation for the number of orthoexcitons. It is assumed that the number of orthoexcitons is small in comparison with the number of paraexcitons, i.e., there are no terms involving collisions between two orthoexcitons or between an orthoexciton and a paraexciton. This is a reasonable assumption in steady state because the orthoexciton down-conversion rate is much more rapid than the paraexciton decay rate.

Now consider the region of the potential well. The equations for this region are virtually identical to those above with the exception of the generation term. The source term of paraexcitons is assumed to be from drifting into the well, at a rate G_p, which is assumed proportional to N_p. Let n_0 and n_p be the number of orthoexcitons and paraexcitons in the well. The rate equations for the well region are then

$$\frac{\partial n_p}{\partial t} = G_p - \frac{n_p}{\tau_p} - an_p^2 + \frac{n_0}{\tau_{DC}} , \tag{23a}$$

$$\frac{\partial n_0}{\partial t} = \frac{n_0}{\tau_{DC}} + \frac{a}{2}n_p^2 . \tag{23b}$$

Again, the number of orthoexcitons is assumed small compared to the number of paraexcitons in steady state. Solving Eqs. (22) and (23) for the number of paraexcitons in steady state yields

$$N_p = \frac{1}{a\tau_p}[-1 + (1 + 2aG\tau_p^2)^{1/2}] , \tag{24a}$$

$$n_p = \frac{1}{a\tau_p}[-1+(1+2aG_p\tau_p^2)^{1/2}] \,. \qquad (24b)$$

In steady state, Eq. (23b) shows that n_0 is proportional to n_p^2. Assuming $G_p = cN_p$, where c can be thought of as the well capture rate, one obtains

$$n_p = \frac{1}{a\tau_p}(-1+\{1+2c\tau_p[-1+(1+2aG\tau_p^2)^{1/2}]\}^{1/2}) \,,$$
$$\qquad (25a)$$

$$n_0 = \frac{a\tau_{DC}}{2}n_p^2 \,. \qquad (25b)$$

The solid curve marked 1 in Fig. 12 is Eq. (25a) with $\tau_p = 0.5$ μsec, $a = 0.05$ sec^{-1}, and $c = 1 \times 10^6$ sec^{-1}. The value of τ_p is determined by a low-power decay-time measurement to be described below. The parameters a and c are both allowed to vary initially. It is found that the shape of the curve is more sensitive to the value of a than that of c.

One can independently estimate the value of c in the following manner. The product cN_p is the number of paraexcitons per unit time flowing into the well. The number which reach the well is of order $N_p\exp(-t_{transit}/\tau_p)$, with $t_{transit}$ equal to the amount of time a particle takes to reach the well from the pumped region of the crystal. This gives

$$c = [\exp(-t_{transit}/\tau_p)]/\tau_{transit} \,.$$

Now $t_{transit} = \Delta x/v_d$, where Δx, the distance traveled, is approximately 0.4 mm, and v_d, the drift velocity, is approximately 1×10^5 cm/sec. This yields $c \approx 1 \times 10^6$ sec^{-1}. The parameter c is fixed at this value and the parameter a is varied to give a reasonable fit to the data. The line marked 2 is Eq. (25b) with the adjustment of an overall multiplier to give the appropriate vertical scale.

The nearly $P^{1/4}$ behavior of the paraexciton intensity in the data described above is due to an Auger decay process at two different regions of the crystal. If one were to create the excitons directly in the well area, one region is eliminated and the power dependence of the paraexciton intensity should be $P^{1/2}$. This is seen by assuming $G_p \propto P$ in Eq. (24b). Shown in Fig. 13 is the extracted density of
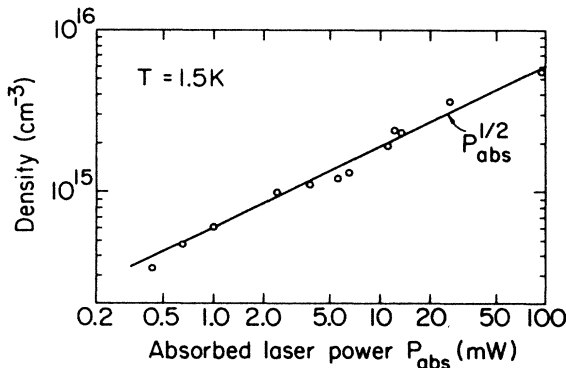
paraexcitons in the well when the laser is pumping the well area directly. This data shows the predicted $P^{1/2}$ dependence. (The corresponding orthoexciton intensity data were not taken at that time.) Thus, the data from this simpler pumping configuration also support the basic rate equations we have used.

Another test of this model is provided by the transient decay of the two types of excitons. Shown in Fig. 14 are time decays of the orthoexciton and paraexciton signals after resonant creation of orthoexcitons at the "bottom" of the well (i.e., the laser was tuned to the orthoexciton quadrupole resonance at the SSM). The dye laser was cavity-dumped. After an initial fast decay, the orthoexciton signal decays at twice the rate of the paraexciton signal. This is consistent with the auger decay mechanism, as can be seen by substituting into Eqs. (22) a solution of the form $N = N^0\exp(-t/\tau_{eff})$ for both the orthoexciton and paraexciton number (a different τ_{eff} for each). The generation rate G is zero at times after $t = 0$. With the additional information that τ_{DC} is of order a few nanoseconds,[16] and that the measured decay times are a few tens to hundreds of nanoseconds, τ_{DC} can then be ig-
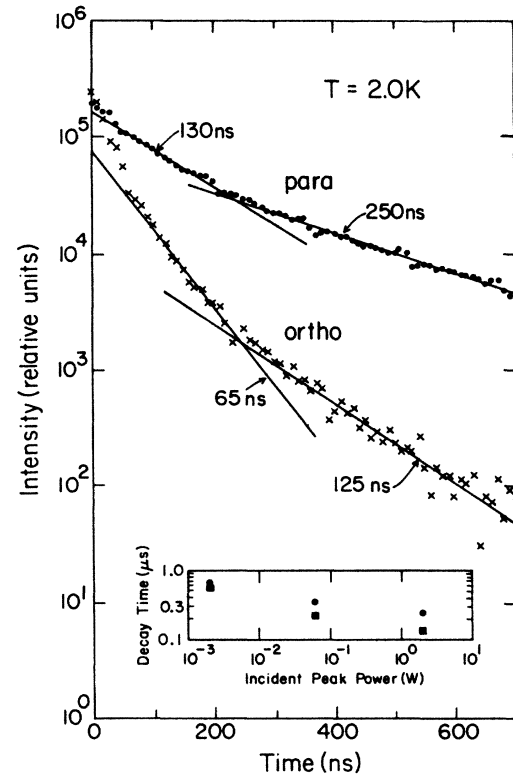

FIG. 14. Intensity of orthoexciton and paraexciton luminescence as a function of time after resonant creation of orthoexcitons at the shear-stress maximum with a cavity-dumped dye-laser pulse. The decays are nonexponential. After an initial fast decay the orthoexciton signal decays at twice the rate of the paraexciton signal. The lines through the data are labeled with the corresponding $1/e$ times. Shown in the inset are the fast (solid squares) and the slow (solid circles) decay times of the paraexciton signal as a function of incident peak laser power. Note that as the power is lowered, the decay seems to become much more exponential, i.e., one decay time.

FIG. 13. Estimated density of paraexcitons as a function of absorbed laser power when exciting the well area directly. The $P_{abs}^{1/2}$ dependence is consistent with the Auger decay mechanism proposed in the text.

nored in comparison to τ_{eff} for the orthoexcitons. This easily yields the results that the decay time for the paraexcitons should be twice that of the orthoexcitons.

The inset of Fig. 14 shows the measured paraexciton decay times for three incident powers. Estimation of absorbed power is impossible because of the pumping configuration. Both the initial and the later decay times are given. The decay times decrease as the power is lowered, as expected for an Auger loss mechanism. At the lowest power, there is little difference between the fast and the slow decay times. It is this low-power decay curve which is the source of the value of τ_p used above.

VI. THERMALIZATION OF EXCITONS IN A PARABOLIC WELL

A basic question that is raised by all the above data is whether paraexcitons energetically and spatially thermalize in the parabolic well. To gain more insight into what is happening, time-resolved spectra and spatial profiles were taken under various excitation conditions. Before discussing data taken from the well area, contrasting data taken under higher-powered pulsed excitation with no stress applied to the crystal will be discussed briefly.

Shown in Fig. 15 are some time-resolved spectra of the phonon-assisted paraexciton line following pulsed excita-

tion of the crystal at a bath temperature of 2 K. The peak incident power was about 3 W and the pulse length was about 15 nsec (cavity-dumped dye laser). The laser was tuned into the phonon-assisted orthoexciton absorption band with an absorption length of about 0.3 mm. The time $t=0$ corresponds to the peak of the laser pulse. Theoretical fits to the spectra are an $E^{1/2}\exp(-E/k_BT)$ Maxwell-Boltzmann distribution with temperature as a variable parameter. The fit temperatures are shown at the left. Note that the paraexcitons display a nearly thermalized distribution of particle energies at short delay times after the intense laser pulse.

Now consider data taken from the well under rather mild excitation conditions. The laser was tuned to the orthoexciton quadrupole resonance at the SSM ("bottom" of the well). The incident peak power was about 0.5 W. Estimation of the absorbed power was impossible because of the pumping configuration, but it should be a very small fraction of the incident power due to the weakness of the quadrupole transition and the short distance over which the absorption takes place. Shown in Fig. 16(a) are
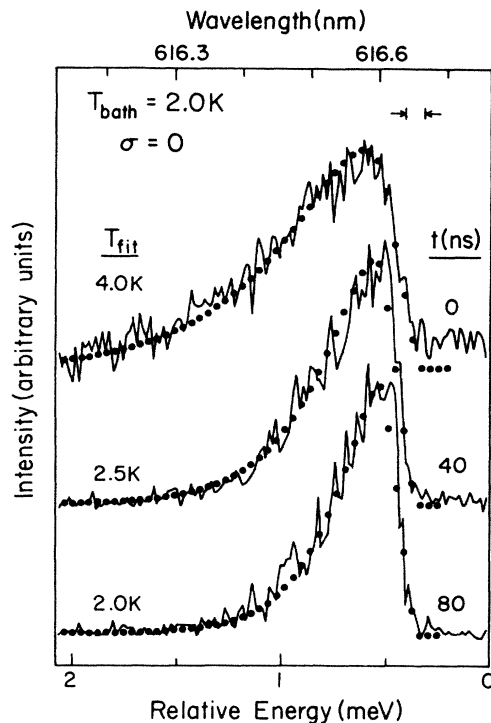

FIG. 15. Time-resolved spectra of the phonon-assisted paraexciton line with no stress applied to the crystal and intense cavity-dumped dye-laser, near-surface excitation. The fits to the data (solid circles) are a Maxwell-Boltzmann distribution $E^{1/2}\exp(-E/k_BT)$ convolved with the resolution function shown in the upper right-hand corner. Fit temperatures are shown at the left with the delay time t given at the right ($t=0$ defined as near the center of the laser pulse). Note that the excitons display a near-thermal distribution of particle energies at short delay times after the laser pulse.
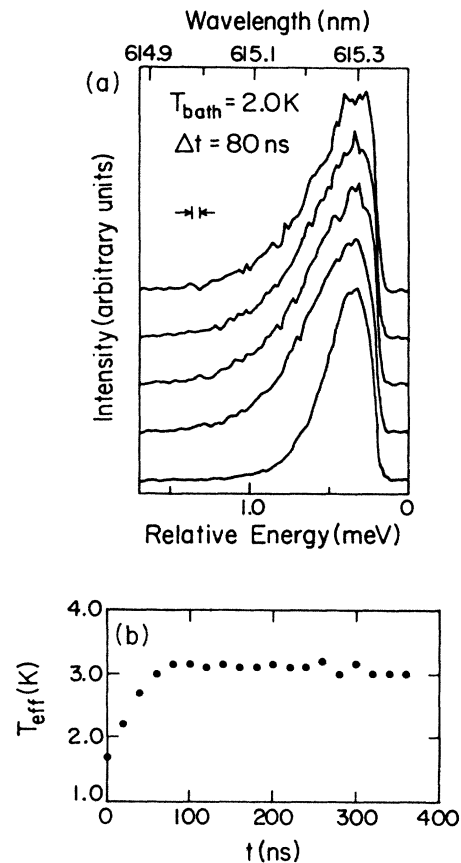

FIG. 16. (a) Time-resolved spectra of the no-phonon paraexciton line after resonant creation of orthoexcitons at the shear-stress maximum. There is an 80-nsec delay between displayed spectra, with the bottom spectrum at the earliest time. (b) An effective temperature extracted from the full width at half maximum of the spectra in (a) assuming a standard $E^{1/2}\exp(-E/k_BT_{eff})$ form for the line shape. As the paraexcitons expand to fill the well, the luminescence line shape broadens correspondingly. $t=0$ is near the peak of the laser pulse.

the resulting time-resolved spectra. The time delay between displayed spectra is 80 nsec. At early times the spectra are narrow due to the narrowness of the spatial distribution. As the excitons diffuse outward to fill the well, the spectra broaden correspondingly. Shown in Fig. 16(b) is an effective temperature, which is a measure of the width of the spectrum, as a function of time. This effective temperature was obtained by assuming a simple $E^{1/2}\exp(-E/k_B T_{eff})$ line shape which yields $1.8k_B T_{eff}$ for the value of the FWHM. No attempts were made to correct for the stress-dependent intensity of the paraexciton no-phonon transition. The feature of note is that at later times the excitons seem to exhibit an effective temperature higher than that of the bath, and the thermalization seems to be very slow. This is in direct contrast to the more rapid thermalization observed at zero stress (Fig. 15).

Shown in Fig. 17(a) are time-resolved spatial profiles taken under virtually identical experimental conditions as above. Again, the time delay between displayed profiles is 80 nsec. Initially, the spatial distribution has a narrow width as determined by the size of the laser beam. As the excitons diffuse outward to fill the well, the width grows. Shown in Fig. 17(b) is the square of the FWHM, Δ, as

I(x)

(a)   T=2.0K
                       Δt=80 ns

⊢ ⊢

←Δ→

-0.2   -0.1   0   0.1   0.2
              x (mm)

0.02

(b)

Δ² (mm²)

0.01
                    • Expt
                    — Theoretical
                       fit to data
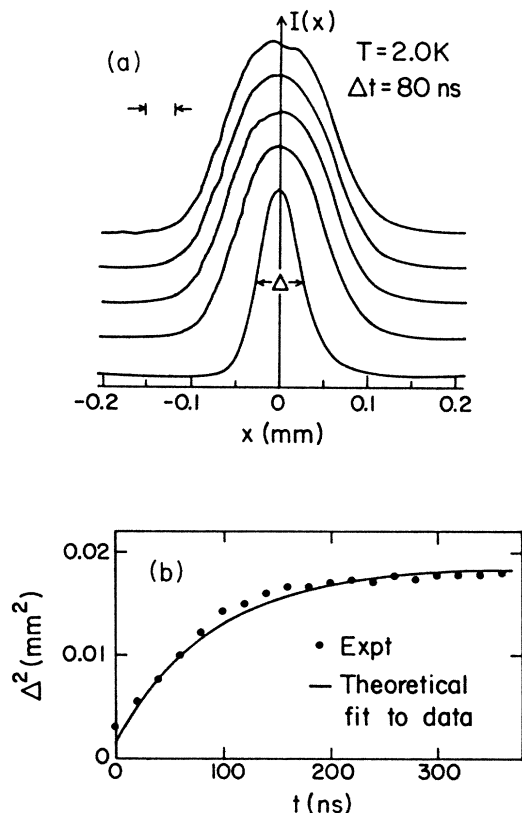
0   100   200   300
              t (ns)

FIG. 17. (a) Time-resolved spatial profiles of no-phonon paraexciton luminescence intensity, $I(x)$, after resonant creation of orthoexcitons at the shear-stress maximum. There is an 80-nsec delay between displayed profiles. (b) Square of the full width at half maximum, Δ^2, as a function of time. The solid line is a fit of Eq. (28) to the data with the parameters $D=190$ cm²/sec, $\gamma=5.6\times10^6$ sec⁻¹, and a "zero" of time of about 7 nsec before the peak of the laser pulse (see text).

function of time. The width of the spatial profile does decrease slightly at longer times, possibly indicating a cooling process.

One can model this diffusivelike expansion process by assuming that the mean free path of excitons between collisions with phonons is small compared to the macroscopic dimension of the potential well. This allows one to model the external potential as providing a spatially varying motive force on the excitons which determines a "local" drift velocity. Along one dimension, an external potential of ax^2 gives a force, $F(x)=-2ax$. This results in a "local" drift velocity, $v(x)=F(x)\tau/m^*$, where τ is the phonon scattering time. Particle conservation, with a sink due to the finite lifetime of the excitons, then yields the following differential equation,

$$\frac{\partial n}{\partial t}=D\frac{\partial^2 n}{\partial x^2}+\gamma n+\gamma x\frac{\partial n}{\partial x}-\frac{n}{\tau_l}\ ,\qquad(26)$$

where $\gamma=2a\tau/m^*$, $n=n(x,t)$ is the local "density" of particles, D is the diffusion constant, and τ_l is the particle lifetime. The solution to this equation, which is a δ function at $x=0$, $t=0$, is

$$n(x,t)\propto\frac{1}{[4\pi(D/2\gamma)(1-e^{-2\gamma t})]^{1/2}}$$
$$\times\exp\left[\frac{-x^2}{4(D/2\gamma)(1-e^{-2\gamma t})}\right]e^{-t/\tau_l}\ .\qquad(27)$$

The FWHM of this distribution is given by

$$\Delta^2(t)=2.77(4)\frac{D}{2\gamma}(1-e^{-2\gamma t})\ .\qquad(28)$$

The solid line in Fig. 17(b) is a fit of Eq. (28) to the data allowing D, γ, and the "zero" of time to vary. (This is required because the spatial distribution has a finite size when created by the laser.) The resultant parameters are given in the figure caption. A value of $D=190$ cm²/sec is obtained from the fit. This is reasonably consistent with the measured[15] drift mobility of paraexcitons at a lattice temperature of 2 K and at a high applied stress. Specifically, $\mu=7.5\times10^5$ cm²/eV sec implies $D=130$ cm²/sec from $D=\mu k_B T$.

Finally, experiments have been performed at the highest paraexciton densities possible with the apparatus. The laser wavelength and spatial position are adjusted to give the maximum no-phonon paraexciton signal from the well. The optimal excitation configuration is very similar to that used to obtain the potential-well luminescence line shapes described in Sec. IV. The differences are that the laser wavelength is shorter, resulting in an absorption region nearly the width of the sample, and the vertical position of the pump beam is closer to the well area. Maximum available cavity-dumped dye-laser power is used, about 5 W peak incident on the sample. The fraction of absorbed power is in the range 10–20 %, as determined from transmission measurements in similar configurations.

Shown in Fig. 18 are time-resolved spectra taken from the well area under these extreme excitation conditions. The time delay between displayed spectra is 80 nsec. The very strange shape of the spectra at early times (bottom
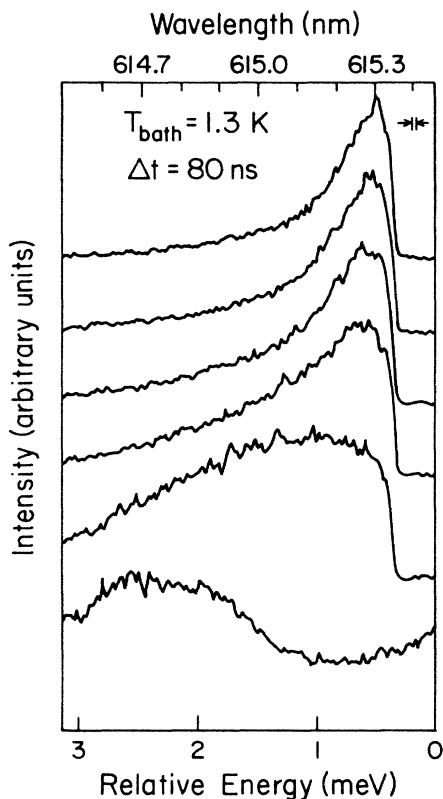
Wavelength (nm)

FIG. 18. Time-resolved spectra of the no-phonon paraexciton line emitted from the well area while pumping horizontally below the potential well with fairly intense laser excitation. The excitons drift into the well. There is an 80-nsec time delay between displayed spectra with the earliest time at the bottom. The strange shape of the spectra at early times is due to the decay of particles on their way into the well. Even for the latest time displayed, the spectrum displays a distribution much hotter than the bath temperature.

spectrum) is due to paraexcitons decaying on their way into the well. Since they decay in a region of the crystal at a lower stress, the emitted light will be of higher energy. Note the long time (~200 nsec) it takes the excitons to finally arrive in the well and display a Maxwellian line shape. This is interpreted as due to a true lattice heating at these high powers. Similar data at a factor-of-30-lower power shows a much more rapid arrival in the well, thus displaying a Maxwellian line shape at earlier times. There still seems to be a slow thermalization taking place. The effective temperature of the top spectrum in Fig. 18 as determined from its FWHM is about 3.5 K at a bath temperature of 1.3 K.

The data described in this paper show a rather slow thermalization of paraexcitons in a stress-induced parabolic potential well. The time-resolved spatial profiles indicate that the excitons are able to "fill" the well in times ≲ 200 nsec, due to their rather large diffusion constant. However, the effective temperature derived from the spectral distribution remains 1−3 K above the lattice temperature over the lifetime of the particle, with the amount of heating dependent on excitation power. In contrast, when no stress is applied to the crystal, the paraexcitons

thermalize much more quickly, even under fairly high laser excitation. What is the major difference between these two situations?

It is known that external uniaxial stress causes the energy separation between the paraexciton and the down-shifted component of the orthoexciton to decrease, and paraexcitons are produced by the down-conversion of orthoexcitons. Ortho-para down-conversion has been studied to some extent,[7,16,20] but there is still no consensus as to the exact processes involved. With no stress applied, 96 cm^{-1} (12 eV) of energy must be given off during the down-conversion. This may occur via the emission of an 87-cm^{-1} optical phonon of symmetry Γ_{25}^- and an acoustic phonon.[20] However, the predicted temperature dependence for the rate of this process was not observed by Weiner et al.[16]

The participation of this 87-cm^{-1} optical phonon may still provide a key to explaining the difference in stress and unstressed thermalization times. When a stress of only about 1 kbar is applied to the crystal, the energy separation between the paraexciton and the down-shifted orthoexciton levels becomes less than 87 cm^{-1}, which could alter the down-conversion process, possibly resulting in a hotter initial distribution of paraexcitons which must then thermalize down to the lattice temperature.

VII. SUMMARY AND CONCLUSIONS

Excitons in a direct-gap semiconductor have been successfully strain-confined for the first time. In contrast to the cases of the indirect-gap materials Si and Ge, where the potential well arises from a splitting of a degenerate conduction band, here the stress-induced potential well at the SSM is due to an interaction between the valence bands causing the symmetry-lowering component of the applied stress to be the dominating factor.

Specific predictions are made for the luminescence line shapes and spatial profiles of luminescence emitted by strain-confined excitons. It is found that as the system of excitons is allowed to become quantum degenerate, the phonon-assisted line gives little indication of the occurrence of the Bose degeneracy; however, the no-phonon line should show significant changes with the approach towards degenerate Bose statistics. For this reason, the existence of a no-phonon transition, such as is the case in a direct-gap semiconductor, may prove quite beneficial when trying to observe quantum-statistical behavior for excitons in a parabolic well.

Spectral line shapes of paraexciton luminescence emitted from the well area for both the no-phonon and the phonon-assisted lines of Cu_2O have been studied. Discrepancies between fit temperatures of the no-phonon and the phonon-assisted lines are found under the assumption of a simple line-shape theory and Maxwell-Boltzmann statistics for the decaying excitons. On the other hand, both the direct and phonon-assisted paraexciton luminescence line shapes could be accounted for with the same effective temperature in the simple line-shape theory by invoking Bose degeneracy of the decaying paraexcitons. However, the estimated densities were much too low, invalidating this assumption. A plausible

alternate explanation incorporates the stress dependence of the paraexciton no-phonon transition and yields consistent results in the limit of classical statistics. There was a good correspondence between the measured no-phonon line shapes and spatial profiles.

The intensity of orthoexciton and paraexciton luminescence emitted from the well region was also studied as a function of laser power. This sublinear behavior was attributed to an Auger decay mechanism resulting from collisions among the paraexcitons. Due to the thermalization of the free electron and hole created in the Auger decay process, there was an additional source of orthoexcitons; hence, the appearance of orthoexciton signal in the well even if the excitation source was located at a large distance from the well.

Lastly, time-resolved data were presented which explored the thermalization of paraexcitons in the parabolic well under various excitation conditions. Even under fairly mild excitation conditions there seemed to be a very slow thermalization taking place. This was contrary to the more rapid thermalization observed for the paraexcitons in crystals with no stress applied. Also, under intense laser excitation, significant lattice heating occurred.

In attempting to achieve Bose-Einstein condensation of long-lived paraexcitons in Cu$_2$O, we have thus encountered two barriers. The principal one is the limitation of exciton density due to Auger collisions even at quite small particle densities ($\geq 10^{14}$ cm^{-3}). A secondary barrier is the rather slow thermalization of excitons in the well. These formidable difficulties must be surmounted before Bose-Einstein condensation of long-lived paraexcitons confined to a strain well can be realized in Cu$_2$O.

ACKNOWLEDGMENTS

*Present address: Kodak Research Laboratories, Eastman Kodak Company, 1999 Lake Avenue, Rochester, NY 14650.

[1]For a review of the properties of electron-hole droplets, see, e.g., J. C. Hensel, T. G. Phillips, G. A. Thomas, and T. M. Rice, in Solid State Physics, edited by H. Ehrenreich, F. Seitz, and D. Turnbull (Academic, New York, 1977), Vol. 32; C. D. Jeffries and L. V. Keldysh, Electron-Hole Droplets in Semiconductors, in Modern Problems in Condensed Matter Physics, edited by V. M. Agronovich and A. A. Maradudin (North-Holland, Amsterdam, 1983), Vol. 6.

[2]L. L. Chase, N. Peyghambarian, G. Grynberg, and A. Mysyrowicz, Phys. Rev. Lett. 42, 1231 (1979); N. Peyghambarian, L. L. Chase, and A. Mysyrowicz, Phys. Rev. B 27, 2325 (1983).

[3]V. B. Timofeev, V. D. Kulakovskii, and I. V. Kukushkin, in Proceedings of the 16th International Conference on the Physics of Semiconductors, edited by M. Averous (North-Holland, Amsterdam, 1983), p. 327.

[4]A. Mysyrowicz, J. Phys. (Paris) Colloq. 41, Suppl. No. 7, C7-281 (1980).

[5]D. Hulin, A. Mysyrowicz, and C. Benoit à la Guillaume, Phys. Rev. Lett. 45, 1970 (1980).

[6]H. Haug and H. H. Kranz, Z. Phys. B 53, 151 (1983).

[7]A. Mysyrowicz, D. Hulin, and A. Antonetti, Phys. Rev. Lett. 43, 1123 (1979).

[8]We thank C. Benoit à la Guillaume for pointing out to us that the spectral line shape of exciton luminescence will be different for these two cases, a fact which we did not recognize in a preliminary account of this work [Phys. Rev. B 28, 3590 (1983)].

[9]See, for example, Charles Kittel and Herbert Kroemer, Thermal Physics, 2nd ed. (Freeman, San Francisco, 1980).

[10]P. L. Gourley and J. P. Wolfe, Phys. Rev. B 24, 5970 (1981); J. P. Wolfe and C. D. Jeffries, in Electron-Hole Droplets in Semiconductors, edited by C. D. Jeffries and L. V. Keldysh, in Vol. 6 of Modern Problems in Condensed Matter Sciences, edited by V. M. Agranovich and A. A. Maradudin (North-Holland, New York, 1983).

[11]R. S. Markiewicz, J. P. Wolfe, and C. D. Jeffries, Phys. Rev. B 15, 1988 (1977).

[12]A. Mysyrowicz, D. P. Trauernicht, J. P. Wolfe, and H.-R. Trebin, Phys. Rev. B 27, 2562 (1983).

[13]R. G. Waters, F. H. Pollak, R. H. Bruce, and H. Z. Cummins, Phys. Rev. B 21, 1665 (1980).

[14]E. F. Gross, F. I. Kreingol'd, and V. L. Makorov, Pis'ma Zh. Eksp. Teor. Fiz. 15, 383 (1972) [JETP Lett. 15, 269 (1972)].

[15]D. P. Trauernicht and J. P. Wolfe, Phys. Rev. B 33, 8506 (1986).

[16]J. S. Weiner, N. Caswell, P. Y. Yu, and A. Mysyrowicz, Solid State Commun. 46, 105 (1983).

[17]F. I. Kreingol'd and V. L. Makarov, Fiz. Tekh. Poluprovodn. 8, 1475 (1974) [Sov. Phys.—Semicond. 8, 962 (1975)].

[18]P. L. Gourley, Ph.D. thesis, University of Illinois at Urbana-Champaign, 1980 (unpublished).

[19]A. Mysyrowicz, D. Hulin, and C. Benoit à la Guillaume, J. Lumin. 24-25, 629 (1981).

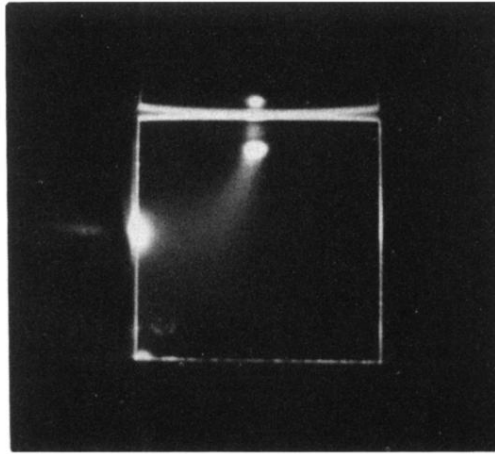[20]N. Caswell and P. Y. Yu, Phys. Rev. B 25, 5519 (1982).

FIG. 5. Photograph of a Cu_2O crystal with stress applied by a glass plunger. An argon-ion laser excites the surface of the sample. The created excitons drift in the stress gradient to the shear-stress maximum where they are confined. This region is the bright spot near the top of the sample. The luminescence seen above the sample is due to a reflection from the glass plunger. The sample dimensions are $1.5 \times 1.5 \times 1.5$ mm^3.